Lab Notes

Editors

Thomas M. Moses | Shane F. McClure
Sally Eaton-Magaña | Artitaya Homkrajae

DIAMONDS

Color-Treated Purple Diamond Rough with Interesting Growth Pattern

Recently, GIA's Dubai laboratory received a purple diamond rough submitted for an identification report, weighing 3.93 ct and measuring 10.26 × 6.82 × 6.05 mm (figure 1). Fourier-transform infrared spectroscopy confirmed this diamond as type Ib with single substitutional nitrogen atoms (N_s^0) of approximately 5 ppm, with characteristic peaks at 1130 and 1344 cm^{-1}. The visible/near-infrared absorption spectrum showed features at 637 nm (NV^-) and 741 nm (GR1). The combination of intense bodycolor, diamond type, and NV centers immediately raised suspicion for color treatment, which ultimately proved to be a combination of irradiation and subsequent annealing. Several noteworthy cases of laboratory-grown polished diamonds color treated to orange to pink hues have been reported by GIA (Summer 2015 Lab Notes, pp. 182–183; Winter 2023 Lab Notes, pp. 489–490), and such post-growth treatment is common in the trade. To the best of the author's knowledge, however, naturally grown rough diamonds color treated to a vibrant purple color description are not commonly submitted for identification reports.

Figure 1. This 3.93 ct diamond rough was color treated to introduce its vibrant purple color. Photo by Nick "Ka Chun" Chan.

DiamondView images revealed interesting patterns that provided additional details on its growth history. Under deep-ultraviolet (UV) illumination (<230 nm), a dark non-fluorescing area resembling an arrow pointing toward a profile view of an elongated diamond was observed (figure 2). The rest of the diamond fluoresced a bright orange, which was likely associated with nitrogen vacancy ($NV^{0/-}$) defects (K.S. Byrne et al., "Photochromic charge transfer processes in natural pink and brown diamonds," *Journal of Physics: Condensed Matter*, Vol. 26, No. 3, 2014, article no. 035501). This distinct pattern indicated that several growth sectors were formed during the diamond's natural growth processes.

Impurities are usually heterogeneously distributed among different growth sectors due to their varying incorporation efficiencies and sector growth rates. Experiments have shown nitrogen concentration is typically higher in the {111} growth sector than in {100} (R.C. Burns et al., "Growth-sector dependence of optical features in large synthetic diamonds," *Journal of Crystal Growth*, Vol. 104, No. 2, 1990, pp. 257–279). Upon irradiation followed by annealing, the pairing of N_s^0 with vacancies to form NV centers becomes significantly more abundant in the {111} sector than in {100}. Photoluminescence spectroscopy further confirmed that {111} was predominated by the negatively charged NV defects (NV^-), while {100} was dominated by the neutral form (NV^0). The 575 nm (NV^0) and 637 nm (NV^-) peak areas in the {111} orange fluorescing areas, normalized to diamond Raman area, were also found to be 7 to nearly 140 times higher than in the {100} dark non-fluorescing region, respectively. The uneven coloration of the treated rough, as seen in visible light, also coincided with the observed differences in the distribution of NV centers between the {111} and {100} sectors (figure 3).

Editors' note: All items were written by staff members of GIA laboratories.

Gems & Gemology, Vol. 62, No. 1, pp. 68–77.

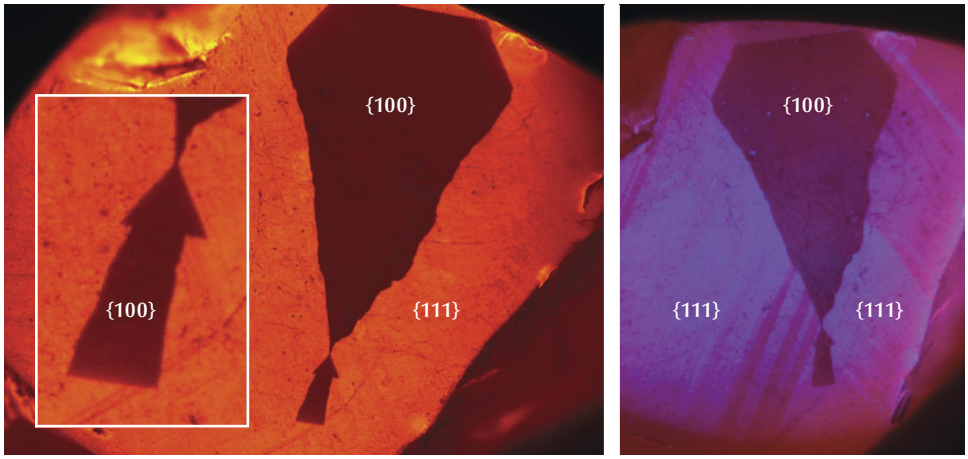

Figure 2. DiamondView images show a dark non-fluorescing region under a standard filter (left; inset shows an enlarged image of the arrow-shaped pattern) and surrounding natural growth patterns using a filter that reduced the NV-related fluorescence relative to other wavelengths (right). Images by Nick "Ka Chun" Chan.

Purple color in diamond is often attributed to transmission windows in the blue and red regions of the visible spectrum. Interestingly, the introduction of NV centers in this stone produced an intense, unmodified purple bodycolor that lacked a pink component commonly observed in diamonds colored with NV centers. Recent studies have shown synthetic type Ib diamonds grown by high-pressure, high-temperature that have undergone high-dose electron irradiation followed by low-temperature annealing of ~750°C can develop an intense purple color within {111} sectors by having predominantly NV^- centers over NV^0. The concentration of NV^- and the intensity of purple bodycolor in those experiments reached a maximum at ~850°C and gradually reduced at higher temperatures (N.M. Kazuchits et al., "Color evolution of type Ib synthetic diamonds after high dose electron irradiation followed by low-temperature annealing," *Diamond and Related Materials*, Vol. 163, 2026, article no. 113334). Based on these observations, it is likely the examined rough underwent a carefully controlled treatment of irradiation followed by annealing at a low temperature.

While arrow facet patterns produced through polishing are often valued, this diamond, however, exhibits pareidolia in the form of an arrow "hidden" from within. It highlights the contrast between distinct growth sectors and is only discernible under deep-UV illumination.

Nick "Ka Chun" Chan

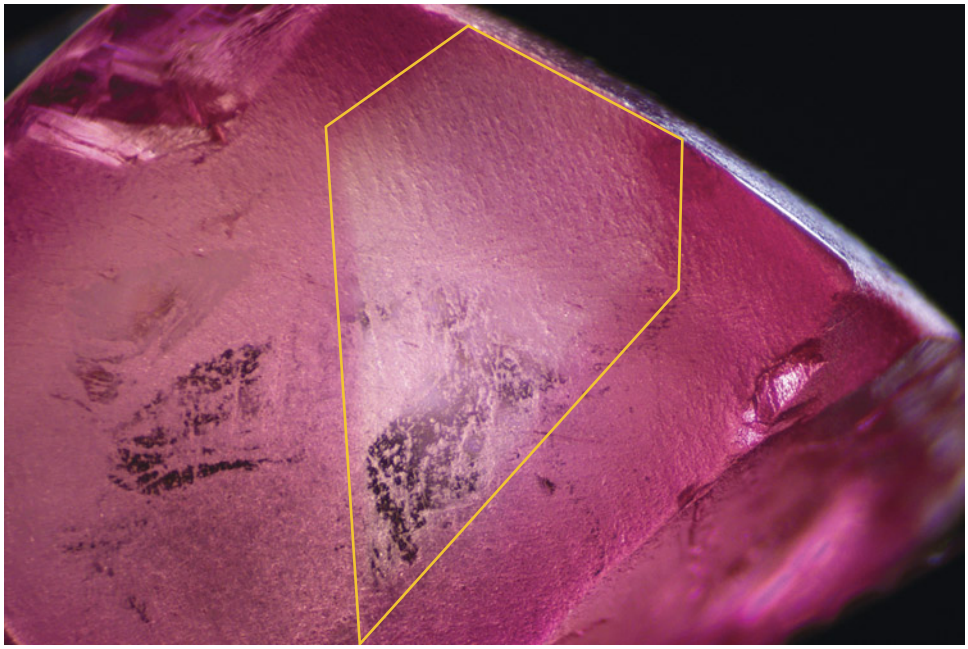

Figure 3. An uneven color distribution is observed under visible light with a distinct boundary resembling a profile view of an elongated diamond (outlined in yellow). Photomicrograph by Nick "Ka Chun" Chan; field of view 7.50 mm.

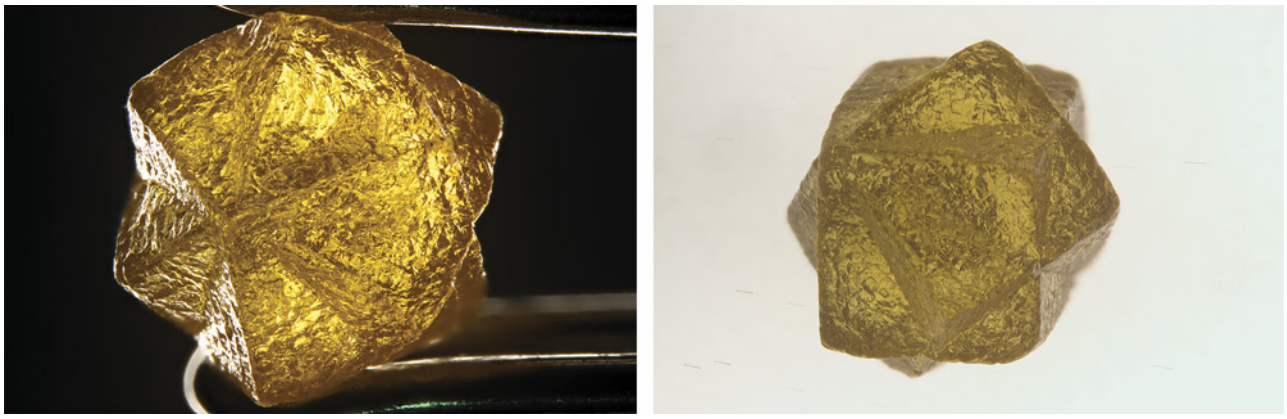

Figure 4. Left: The twinned 0.37 ct diamond displays a vivid orangy yellow color. Right: The intersection of cuboid crystals is clearly observed from this view. Photomicrographs by Taryn Linzmeyer; field of view 7.19 mm.

Interpenetrant Twins in Natural Diamond

A 0.37 ct vivid orangy yellow rough diamond displaying penetration twinning, on loan from the GIA Museum, was recently examined by the author (figure 4). Growth twinning is a natural process involving the symmetrical intergrowth of two crystals of the same mineral. Diamonds can exhibit growth twinning as either contact twins or penetration twins. Contact growth twinning is commonly observed in octahedral diamonds, forming macles (e.g., A. Abduriyim and M. Kitamura, "External morphology and internal zonal structure of macle diamond," Fall 2025 *G&G*, pp. 250–269). Much more rarely, interpenetrant twinning is observed in cuboid diamonds displaying fibrous growth (e.g., K. Sun et al., "Growth and crystallographic features of interpenetrant twins in natural diamonds," *American Mineralogist*, Vol. 110, No. 8, 2025, pp. 1249–1256; J.W. Harris et al., "Morphology of monocrystalline diamond and its inclusions," *Reviews in Mineralogy and Geochemistry*, Vol. 88, No. 1, 2022, pp. 119–166).

Spectroscopic analysis was performed to further characterize the diamond. Ultraviolet/visible spectroscopy revealed a broad absorption continuum primarily in the violet to blue regions of the visible spectrum. This is seen in diamonds colored by isolated substitutional nitrogen atoms (N_s^0) or C-centers. Fourier-transform infrared spectroscopy detected these C-centers in addition to A-centers (paired nitrogen atoms), revealing this stone to be type IaA+Ib.

This natural diamond is an example of how "accidents" during crystal growth can result in fascinating mineral specimens.

Taryn Linzmeyer

EMERALD with Abundant Magnetite Inclusions

Gemologists use several key inclusions to aid in origin determination and to distinguish between naturally grown and laboratory-grown emeralds. Among these, two-phase

Figure 5. Rare multiphase inclusion containing fluid (liquid and gas) and solid phases of magnetite and phlogopite, along with magnetite crystals in four distinct forms (irregular, octagonal, blocky, and dendritic), observed in a 3.03 ct Zambian emerald. Corresponding illustration on the right highlights inclusion details. Photomicrograph by Aprisara Semapongpan; field of view 1.80 mm.

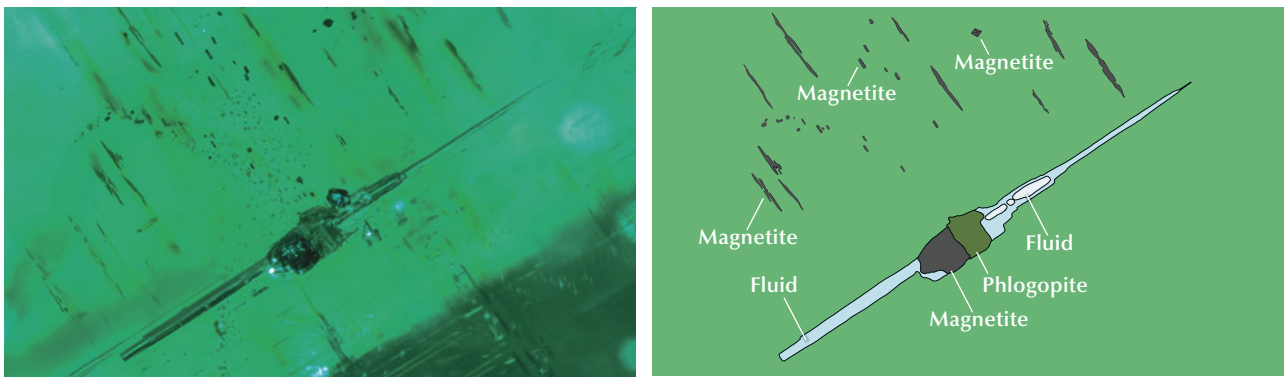

and multiphase inclusions are particularly important. In addition, some characteristic inclusion features are particularly useful for origin determination, such as iridescent two-phase thin films reported in certain Russian emeralds.

Recently, a 3.03 ct natural emerald was submitted to the Bangkok laboratory. Standard gemological testing, characteristic inclusion features, and chemistry supported a Zambian origin. Under the microscope, the stone showed the typical blocky two-phase inclusions expected in Zambian emerald, along with numerous opaque black metallic inclusions of various shapes and rare multiphase inclusions containing liquid, gas, and two solid phases (figure 5). Raman spectroscopy identified the opaque black metallic inclusions as magnetite and the transparent green solid in the multiphase inclusions as phlogopite.

Magnetite inclusions in Zambian emeralds are related to the host rock composition and the metamorphic-metasomatic formation process. Beryllium-rich fluids from pegmatites react with chromium-bearing talc-magnetite schist to form emeralds, which can trap magnetite grains from the surrounding rock (H. Zwaan et al., "Emeralds from the Kafubu area, Zambia," Summer 2005 *G&G*, pp. 116–148). In this stone, magnetite occurred in unusually high abundance and exhibited four distinctive crystal habits. Dendritic or skeletal forms appeared as fine planar networks roughly parallel to the basal pinacoid. Blocky and octagonal crystals formed in more stable growth environments, while irregular crystals indicated more variable growth conditions. The simultaneous presence of all four forms is rarely observed in Zambian emeralds and makes this stone particularly unique.

The abundance of magnetite produced a weak but noticeable attraction to a handheld magnet, an uncommon physical response in emeralds. This observation, together with the inclusion assemblage and chemical data, supports a Zambian origin and highlights how unusual internal features can reflect natural geological variation.

This emerald expands the reference for Zambian material, showing that magnetite can appear not only as small, scattered grains but also in multiple distinct habits and in high quantities. The combination of abundant magnetite, four crystal forms, magnetic response, and rare multiphase inclusions makes this specimen particularly noteworthy and a fine example of natural variation in Zambian emeralds.

Aprisara Semapongpan

Figure 6. The fashioned dyed shell weighing 17.99 ct and measuring 19.58 × 12.25 mm. Photo by Gourav Bera.

A Fashioned Dyed Shell IMITATION PEARL

Recently, GIA's Mumbai laboratory received a parcel of brown and black non-nacreous pearls for identification. Among these, the largest dark brown drop-shaped specimen, weighing 17.99 ct and measuring 19.58 × 12.25 mm (figure 6), exhibited visual and structural features inconsistent with the other examined pearls.

Externally, the specimen displayed fine banding across its dark brown non-nacreous surface (figure 7A), with an irregular light brown nacre covering one area. Microscopic examination using fiber-optic illumination revealed working and polishing lines on both the nacreous and non-nacreous portions, with the lines more distinct on the nacreous surface (figure 7B). The non-nacreous area showed a mosaic-like cellular pattern, with black concentrated

Figure 7. A: Fine banding in the dark brown non-nacreous areas. B: Distinct grinding and polishing lines on the light brown nacreous surface; field of view 8.60 mm. C: Mosaic-like cellular structure with a black dye residue in the surface-reaching cracks; field of view 3.80 mm. Photos by Gourav Bera (A) and Anukul Belanke (B and C).

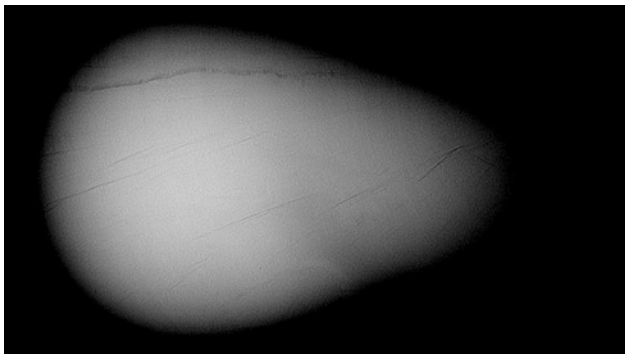

Figure 8. RTX imaging revealing parallel banding. Image by Anukul Belanke.

along the banding and surface fractures attributable to the presence of a dye (figure 7C) (Fall 2021 Lab Notes, pp. 264–266), making it difficult to determine the mollusk species. When exposed to X-ray excitation, the specimen was inert. In addition, chemical analysis using energy-dispersive X-ray fluorescence detected no measurable manganese and a strontium level of 1283 ppm, indicating its saltwater origin.

Under long-wave ultraviolet radiation, the specimen showed a weak greenish yellow reaction on its light brown areas, while darker portions remained inert. Raman spectroscopy using a 514 nm laser on the lighter brown nacreous area produced a doublet at 701 and 704 cm^{-1} and a peak at 1086 cm^{-1}, indicative of aragonite. In contrast, no spectral peaks were detected on the dyed, darker brown non-nacreous area due to high fluorescence interference. Real-time X-ray microradiography (RTX) revealed distinctive internal parallel banding and fine surface-reaching cracks (figure 8), typical of shell material.

Collectively, these observations confirmed that the examined specimen was fashioned out of shell, carefully shaped and polished to imitate the appearance of a non-nacreous pearl, such as those produced from the Pinnidae family (N. Sturman et al., "Observations on pearls reportedly from the Pinnidae family (pen pearls)," Fall 2014 *G&G*, pp. 202–215). The presence of dye, combined with deliberate shaping and polishing, significantly enhanced its resemblance to a natural pearl. With the increasing market presence of imitations, continued caution and thorough analytical examination are essential for ensuring accuracy in pearl identification.

Anukul Belanke, Roxane Bhot Jain, Nishka Vaz, and Abeer Al-Alawi

Chocolate OPAL

Opal is renowned for its wide range of colors, from deep blue to intense red to completely black. All bodycolors are caused either by the presence of nanoscale mineral inclusions or chemical elements incorporated directly into the amorphous silica structure. Aside from their contributions to visual appeal, these color-causing compounds are also of scientific interest, as their presence can provide more precise constraints on the local conditions and environment of opal formation.

Recently, GIA's New York laboratory acquired a collection of various rough Ethiopian opals (Wollo and Shewa provinces) for research purposes, displaying a range of bodycolors from colorless to red-orange (so-called "fire opals"). The collection included an exceptional 37.93 ct common specimen with a 4.05 ct small detached fragment, bearing a striking resemblance to a bar of chocolate (figure 9). Both pieces displayed a lustrous appearance on the conchoidal fracture and homogeneous bodycolor throughout the volume, leaning toward red in thinner parts, with slight

Figure 9. A 37.93 ct chocolate common opal (left) and its 4.05 ct detached fragment (bottom) next to a piece of a chocolate bar (right). Photo by Towfiq Ahmed.

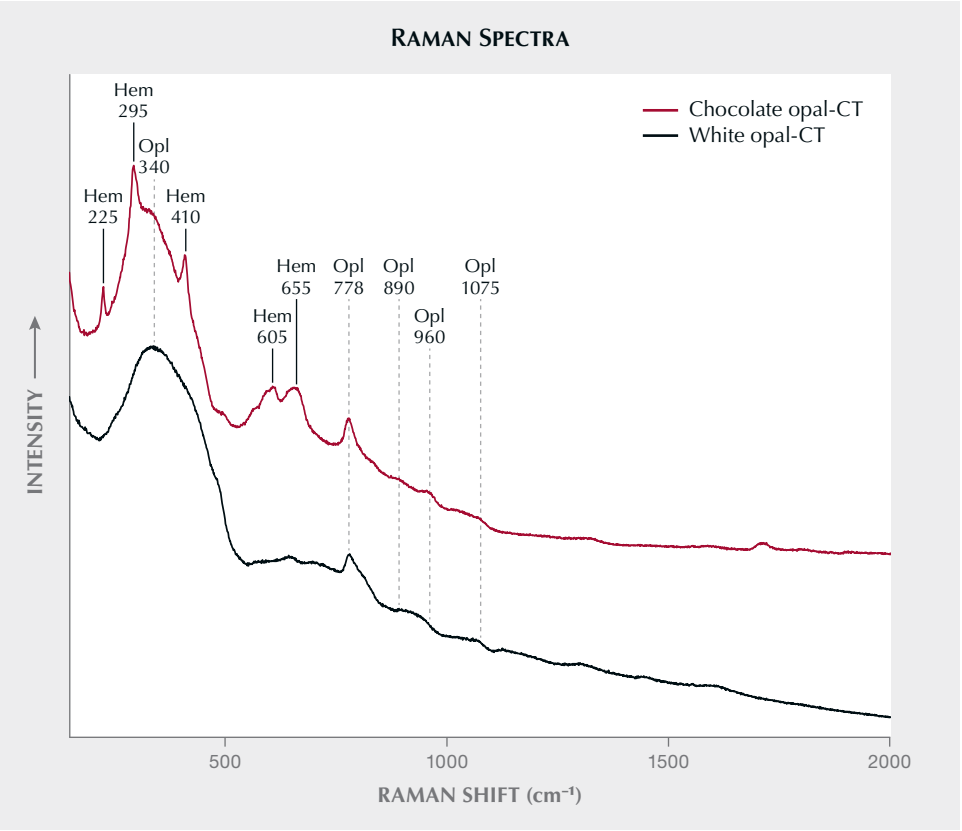

Figure 10. Comparison of the 830 nm Raman spectra of the chocolate common opal and a white common opal from the same Ethiopian deposit. Opl = opal; Hem = Hematite. Spectra are offset vertically for clarity.

variation on the surfaces and localized zones of lighter brown color. Standard gemological testing on the larger piece revealed a specific gravity of 2.00 and a spot refractive index of 1.46, typical for opal.

Raman spectroscopy and laser ablation–inductively coupled plasma–mass spectrometry were performed to better characterize this material. With an 830 nm excitation laser, Raman peaks at 340 and 780 cm^{-1} confirmed the specimen as opal-CT. Faint Raman peaks related to iron oxides were also seen (figure 10). Using a 514 nm laser, the opal signal was almost completely suppressed, enhancing the signal of the iron oxides; these were confirmed as hematite (Fe_2O_3) (figure 11) (C.P. Marshall et al., "Polarized Raman spectra of hematite and assignment of external modes," *Journal of Raman Spectroscopy*, Vol. 51, No. 9, 2020, pp. 1522–1529).

The chemical composition in the major (silicon, oxygen, and water) and main minor elements (sodium, magnesium, aluminum, and calcium) of this chocolate brown specimen falls within the classical range of values established in the literature for the chemistry of Ethiopian opal (B. Rondeau et al., "Geochemical and petrological characterization of gem opals from Wegel Tena, Wollo, Ethiopia: Opal formation in an Oligocene soil," *Geochemistry: Exploration, Environment, Analysis*, Vol. 12, No. 2, 2012, pp. 93–104; B. Chauviré et al., "Pedogenic origin of precious opals from Wegel Tena (Ethiopia): Evidence from trace elements and oxygen isotopes," *Applied Geochemistry*, Vol. 101, 2019, pp. 127–139). However, certain trace elements such as iron, titanium, manganese, zinc,

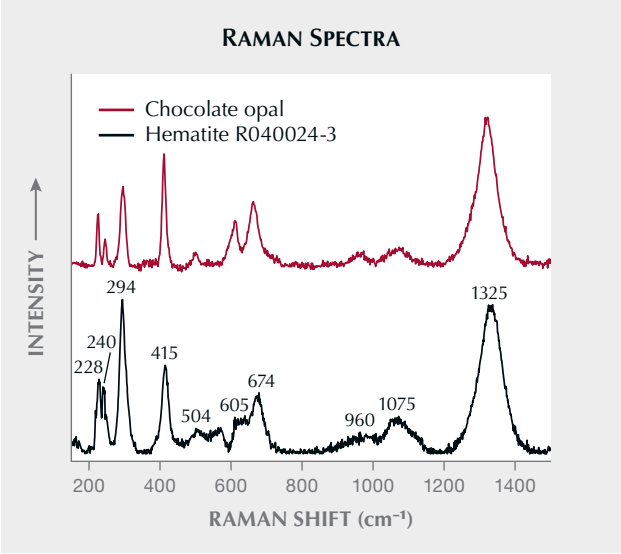

Figure 11. Comparison of the 514 nm Raman spectra of the chocolate opal and hematite reference. Spectra are offset vertically for clarity.

niobium, lead, and thorium are enriched relative to most Ethiopian opals. Furthermore, there is considerable enrichment in the rare earth elements (REEs) in conjunction with a pronounced and unusual positive cerium anomaly.

The strong positive cerium anomaly (463±14 ppm) relative to most Ethiopian opals (<90 ppm), along with the presence of embedded iron oxides, would indicate that this specimen formed under oxidizing conditions. Ethiopian opals are known to form within volcanic tuffs (compacted ash, also called ignimbrite) of rhyolitic composition that have undergone active soil formation processes (also called pedogenesis). Moreover, the presence of fossils in the surrounding rocks and within the opals themselves indicates that their formation environment was also rich in living organisms (and their organic byproducts); recent research has revealed clues toward an active interaction between opal and these organisms (S. Gouzy et al., "Whitening of fire opal: Transformation of silica in soils," *Chemical Geology*, Vol. 616, 2023, article no. 121237). Among other parallel processes that might occur in this complex setting, microbial mediation (i.e., wherein microorganisms facilitate chemical transformations of an environment) has been specifically identified as a possible origin of strong cerium anomalies (B. Chauviré et al., 2019, and references therein) and control overall REE partitioning during opal formation. Therefore, it can be hypothesized that the peculiar chemistry of this opal could be related to an intense, localized microbial activity in its immediate growth environment.

Correlated to the positive cerium anomaly, the chocolate opal is also enriched in europium compared to more common Ethiopian samples. However, this europium enrichment is not accompanied by similarly high concentrations of strontium and barium, a suite previously attributed to feldspar-dominated weathering as the source of chemical elements for opal (B. Chauviré et al., 2019). This suggests that, for this specimen, the predominant source of elements was likely the volcanic glass component of the ignimbrite rather than feldspar phenocrysts.

This specimen stands out among all opals from Ethiopia and around the world, not only for its striking dark chocolate color, but also for its unique chemical composition enriched in REEs and other elements commonly believed to only occur in trace concentrations, such as cerium (usually lower than 90 ppm and here 463±14 ppm). Finally, this peculiar chocolate opal highlights, once again, the high sensitivity of opals to their hyperlocal environmental variations, even within the same deposit.

Simon Gouzy, Sarah Arden, and Tyler Smith

PEARLS

Atypical Bead Cultured Pearls Identified in a Natural Pearl Necklace

Recently, GIA's Mumbai laboratory received a five-strand necklace for identification, consisting of light cream and cream pearls (figure 12, left). The pearls varied in shape from near-button to near-oval, with diameters ranging from 3.27 to 4.80 mm, providing an overall well-matched appearance. Real-time X-ray microradiography (RTX)

Figure 12. Left: Necklace consisting of natural pearls and eight atypical bead cultured pearls. Right: The removed atypical bead cultured pearls from the necklace, ranging in weight from 0.51 to 0.68 ct. Photos by Gourav Bera.

revealed that the majority of pearls were natural, showing different-sized cores surrounded by concentric growth arcs, while some displayed minimal structures. However, eight pearls exhibited suspicious internal structures, with some showing unclear demarcations. These were difficult to conclusively identify in their strung condition and were removed for further analysis (figure 12, right).

The eight removed pearls weighed between 0.51 and 0.68 ct, with sizes ranging from 4.45 × 4.33 × 3.53 mm to 5.30 × 4.22 × 3.98 mm. Energy-dispersive X-ray fluorescence revealed no traces of manganese, with strontium levels ranging from 981 to 1270 ppm, indicating a saltwater growth environment. However, when exposed to X-rays, some of the pearls showed a very weak yellowish green fluorescence and a stronger fluorescence in their drill holes. While saltwater pearls are usually inert to X-ray fluorescence, saltwater bead cultured pearls with freshwater shell nuclei tend to fluoresce with a weak to moderate yellowish green reaction (Fall 2023 Lab Notes, pp. 365–366). The weak fluorescence observed in these saltwater pearls, along with stronger fluorescence in the drill holes, indicated the potential presence of a freshwater nucleus within each pearl.

Detailed analysis of the internal structures via RTX and X-ray computed microtomography (μ-CT) confirmed that each of the eight pearls had a nucleus and boundary structure (figure 13). These nuclei appeared slightly more radiopaque than the surrounding nacre, were asymmetrical in shape, and lacked the growth structure present in the nacre surrounding them. In general, traditional bead cultured pearls are produced with spherical freshwater shell beads, which are easily identifiable through RTX analysis. When these freshwater shell beads are cut into differing shapes, or any other materials are used as nuclei, the resulting pearls are classified as atypical bead cultured (aBC) pearls.

The identification of this type of aBC pearl with an irregularly shaped shell bead presents significant challenges due to its deceptive similarities to the external appearance of natural pearls. Their irregular shape, characterized by asymmetrical and non-traditional nucleation, can mislead both gemologists and consumers alike. This necklace is particularly noteworthy as it marks the first time GIA's Mumbai laboratory has encountered numerous relatively small aBC pearls of this type, drilled and strung alongside natural pearls. As cultivation techniques continue to evolve, the challenges associated with pearl identification will only increase. Therefore, it is essential for gemologists to accurately identify cultured pearls when intermixed with natural pearls of similar appearance.

Nishka Vaz, Karan Rajguru, and Abeer Al-Alawi

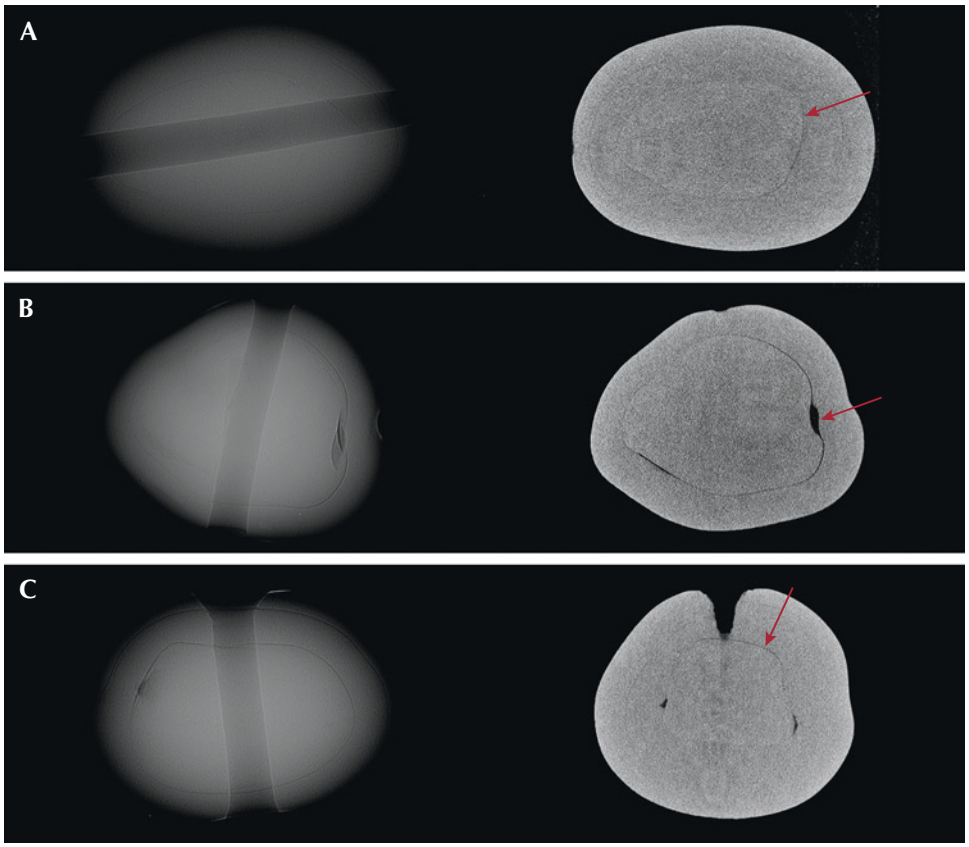

Figure 13. RTX (left) and μ-CT (right) images of three of the eight atypical bead cultured pearls. A: A very faint discontinuous demarcation that appears more like a growth structure in the RTX image but shows different radiopacity and a continuous demarcation in the μ-CT image (red arrow). B: A faint demarcation and small void (red arrow). C: A more definite boundary structure (red arrow) and radiopacity difference.

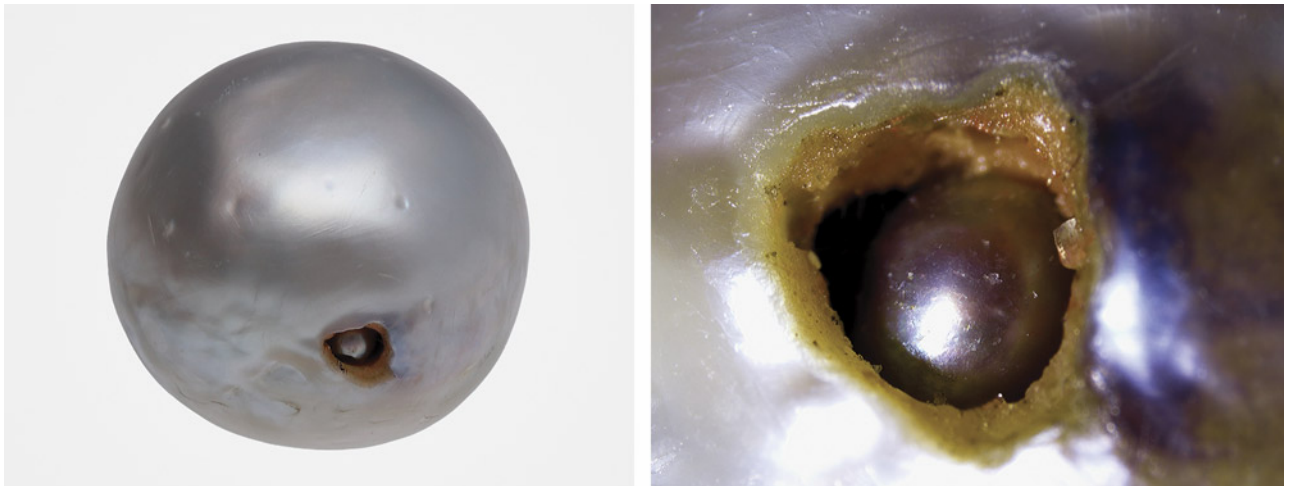

Figure 14. Left: A light gray near-round pearl weighing 13.12 ct and measuring 14.06 × 13.75 × 12.76 mm, plugged with a drilled seed pearl. Right: A closer view of the seed pearl embedded in the pearl's opening. Photos by Gourav Bera (left) and Karan Rajguru (right).

An Unusual Filled Cultured Pearl

Recently, GIA's Mumbai laboratory received a light gray near-round pearl for identification, weighing 13.12 ct and measuring 14.06 × 13.75 × 12.76 mm. Externally, the surface of the pearl displayed an uneven texture with white blotches and had an opening plugged with a small light brownish gray near-round seed pearl (figure 14). Under higher magnification, the surface of both the pearl and the seed pearl revealed typical nacreous structures with overlapping aragonite platelets. The presence of aragonite was further confirmed by Raman spectroscopy using 514 nm laser excitation.

Chemical analysis of the pearl using energy-dispersive X-ray fluorescence revealed no traces of manganese and a strontium level of 1535 ppm. Both the pearl and the seed pearl showed inert reactions when exposed to X-ray fluorescence, confirming their saltwater origins.

Real-time X-ray microradiography (RTX) and X-ray computed microtomography (μ-CT) images both revealed a distinct light gray demarcation of nacre surrounding a large dark gray area of an unidentified radiolucent foreign material within the large pearl (figure 15). The unidentified material contained darker gray blotches of gas bubbles. The seed pearl was seen resting atop the filling material,

Figure 15. RTX (left) and μ-CT (right) imaging reveal a seed pearl at the opening and an unidentified foreign material inside the pearl.

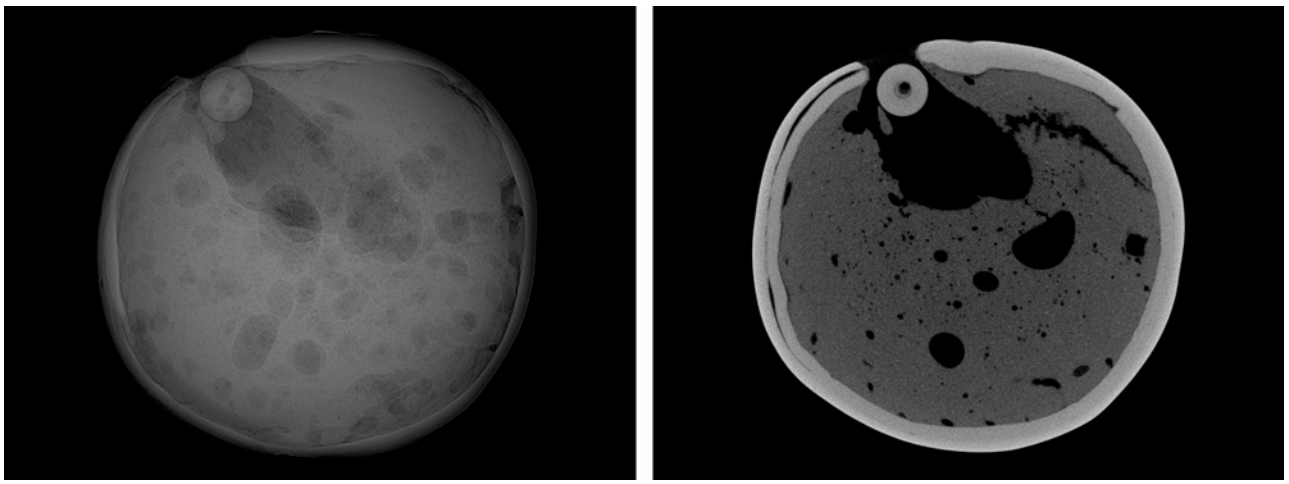

suggesting it was intentionally used to seal the pearl's opening. The drilled seed pearl exhibited a central core surrounded by fine growth arcs similar to those observed in natural pearls.

Two possible scenarios arise regarding the pearl's formation. The first suggests the use of an atypical bead for culturing the pearl, differing from the conventional freshwater shell bead. Numerous experimental attempts have explored alternative materials as bead nuclei, including organic nuclei or, as in this case, an unknown material similar to synthetic substances such as plastic or resin (L. Cartier and M.S. Krzemnicki, "New developments in cultured pearl production: Use of organic and baroque shell nuclei," *Australian Gemmologist*, Vol. 25, No. 1, 2013, pp. 6–13; S.C. Shih and P. Cevallos, "Polystyrene nucleus in a freshwater cultured pearl," *Journal of Gemmology*, Vol. 39, No. 5, 2025, pp. 445–447). The second scenario could be that it was filled after the formation of the pearl. The latter scenario appears more plausible due to the presence of gas bubbles within the void and along the demarcation. This intention to mask the unidentified foreign material with the seed pearl further complicated identification.

Identifying the nature of such a pearl can be challenging, whether it is an atypical bead cultured pearl or a filled non-bead cultured pearl. While the possibility of alternative culturing methods cannot be overlooked, the characteristics observed in the examined pearl suggest that it is not of natural origin but rather a product of a cultured formation. Further analysis is required to understand the composition of the unidentified foreign material and to reach a more conclusive identification of the pearl.

Karan Rajguru, Abeer Al-Alawi, Roxane Bhot Jain, and Artitaya Homkrajae

Transparent STAUROLITE

The Carlsbad laboratory recently received a transparent 1.58 ct dark red-brown freeform step cut measuring approximately 6.24 × 8.08 × 3.56 mm (figure 16). Standard gemological testing results included a specific gravity of 3.76 and a refractive index of 1.738–1.748. These properties suggested the stone was a rare transparent staurolite, which was confirmed by Raman spectroscopy. Typically, staurolite forms as opaque brown to black X- or cross-shaped twin crystals. Due to its typical cross-shaped appearance, the material was named using the Greek word for "cross," *stavros* (J.W. Anthony et al., Eds., *Handbook of Mineralogy*, Mineralogical Society of America, Chantilly, VA, http://www.handbookofmineralogy.org/).

Figure 16. A rare transparent 1.58 ct dark red-brown staurolite. Photo by Santi Jittathai.

Transparent staurolite is extremely rare; this is only the second transparent specimen examined by GIA to date. However, examples of transparent staurolite as an inclusion have been documented in ruby (e.g., Spring 2020 *G&G* Micro-World, pp. 144–145; Fall 2020 *G&G* Micro-World, pp. 434–435).

Michaela Damba